

Negative Feedback Avalanche Diodes for Near-infrared Single Photon Detection

Xudong Jiang*, Mark A. Itzler, Bruce Nyman, Krystyna Slomkowski
Princeton Lightwave Inc., 2555 US Route 130, Cranbury, NJ, USA 08512

ABSTRACT

In recent years significant progress has been made in near-infrared single photon detection using Geiger-mode InP-based single photon avalanche diodes (SPADs). A more detailed understanding of these detectors with regard to device design, material growth and device fabrication has led to continual performance improvements. A variety of circuits for enabling SPAD Geiger-mode operation have been proposed and demonstrated as well. However, due to the inherent positive feedback nature of the avalanche process, Geiger-mode SPADs are constrained by certain performance limitations, particularly with regard to counting rate and the absence of photon number resolution. These limitations hinder the use of SPADs in certain applications. By incorporating a negative feedback mechanism into InP-based SPADs, these SPAD performance limitations can be overcome. In this paper, we present a negative feedback avalanche diode (NFAD), which is formed by monolithically integrating a passive negative feedback element with a high-performance InP-based SPAD. We describe the design and operation of the NFAD device, along with basic characteristics such as pulse response and quenching dynamics, as well as the dependence of these characteristics on excess bias voltage and input photon number. We will also review the results of near-infrared single photon counting performance for fundamental performance parameters such as photon detection efficiency, dark count rate, and afterpulsing.

Keywords: Avalanche photodiodes, single photon detector, SPAD, InGaAsP, negative feedback

1. INTRODUCTION

There is a wide range of applications that require single photon detection in the near infrared (NIR) wavelength range between 1.0 and 1.7 μm , such as optical time domain reflectometry [1], quantum cryptography [2], photon-correlation spectroscopy [3], fundamental studies in quantum physics [4], semiconductor devices and material characterization [5], laser ranging [6], and free space optical communications in photon-starved environments [7]. InP-based single photon avalanche diodes (SPADs) offer the most practical solution due to their performance, compactness, reliability and cost.

The SPAD operates in Geiger mode, where it is biased above its breakdown voltage and the photoexcitation of just a single charge carrier can lead to a self-sustaining avalanche and produce a macroscopic current pulse that can be sensed using an appropriate threshold detection circuit. The counting rate of existing InP-based SPADs is generally limited to the order of 1 MHz, and these detectors do not have the ability to resolve photon number. The relatively low counting rate of InP-based SPADs limits their use in many photon counting applications. Negative feedback avalanche diodes (NFADs) could provide a possible solution to the two principal drawbacks of InP-based SPADs. In NFADs, a resistor with appropriate resistance is monolithically integrated with a SPAD. This monolithically integrated resistor can quench the avalanche quickly and at the same time regulate the charge flow through the device. The number of carriers involved in the avalanche of a typical InP-based SPAD is large ($\sim 10^7 - 10^8$). Whereas in a NFAD, the number of carriers in an avalanche can be reduced to the order of 10^5 . The reduced charge flow inside the NFAD device will significantly reduce the afterpulsing, which is proportional to the total charge flow. The fast quenching and reduced charge flow inside NFAD could significantly increase the device's photon counting rate. This will have immediate impact on many applications, such as quantum cryptography and lidar measurement. Since the charge flow within each device is regulated by the monolithically integrated resistor, when these NFAD devices are aggregated into a matrix

*xjiang@princetonlightwave.com; tel: 1 609 495-2584; www.princetonlightwave.com

format with all devices biased together in parallel, the sum of the matrix output will be proportional to the number of devices fired. Therefore the NFAD array will be able to resolve photon number under certain incident photon flux condition (below the saturation level of the matrix). This will have important implications in certain applications such as quantum computing. From these perspectives, the NFAD will be a very attractive device for many important applications involving NIR single photon detection.

There have been some reports in the literature on the attempt to use negative feedback in APDs, such as using various monolithically integrated resistors in silicon APD for nuclear and particle physics experiment [8,9], and using an epitaxial heterobarrier in InP-based APDs to quench avalanches [10]. Itzler *et al.* reports the first NFADs using InP-based SPADs with monolithically integrated thin film resistors [11]. Though conceptually similar to passive quenching, which to date has been achieved through hybrid integration approaches [12], the NFAD avoids the large parasitic effects involved in typical passive quenching solutions and shows interesting phenomena that cannot be explained by simple passive quenching.

In this paper, we describe the design and characterization of InP based NFADs. In section 2, the design of NFAD device and method for characterizing NFADs are described. In section 3, the characterization results for InP based NFADs are presented. Some discussions on InP based NFAD performance are undertaken in section 4, followed by a summary of conclusions.

2. NFAD DESIGN AND METHOD OF CHARACTERIZATION

To obtain high-performance NFAD devices, the intrinsic performance of the underlying SPAD structure is very important. Efforts have been undertaken at Princeton Lightwave, Inc. to fabricate high-performance SPADs at both 1.06 μm and 1.55 μm [13,14,15]. Figure 1 shows the DCR versus PDE performance of the SPADs used in the NFAD device structure at different operating temperatures.

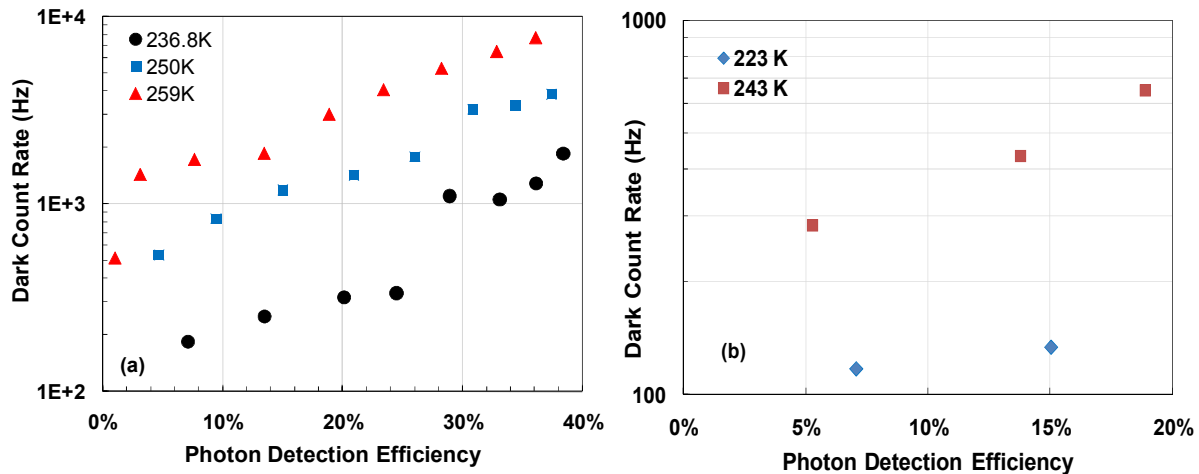


Figure 1 Dark count rate (DCR) versus photon detection efficiency (PDE) for 1.06 μm (a) and 1.55 μm (b) SPADs. In (a), symbols represented by circles, squares and triangles are the experimental results taken at 237K, 250K and 259K, respectively. In (b), the symbols represented by diamonds and squares are experimental results taken at 223K and 243 K, respectively.

The 1.06 μm SPAD data shown in Figure 1(a) is obtained from an 80 μm diameter device. The dark count rate of this device at 30% PDE is ~ 1 kHz at 237 K. The 1.55 μm SPAD data shown in Figure 1(b) is obtained from a 25 μm diameter device, and at 223 K, the dark count rate at 15% photon detection efficiency is less than 150 Hz. Both 1.06 μm and 1.55 μm SPAD show excellent intrinsic performance.

Figure 2 shows the schematic of a test set-up for NFAD device characterization. NFAD is biased above breakdown voltage by a SMU through a bias tee. Avalanche pulses generated inside the NFAD are fed into an amplifier, and the output of the amplifier is connected to a Tektronix digital scope or a Signatec acquisition card. The digital scope has high resolution, but its depth of memory is limited. The resolution of the data acquisition card can reach 1 ns, and can record data for a duration of 0.25 second with 1 ns resolution.

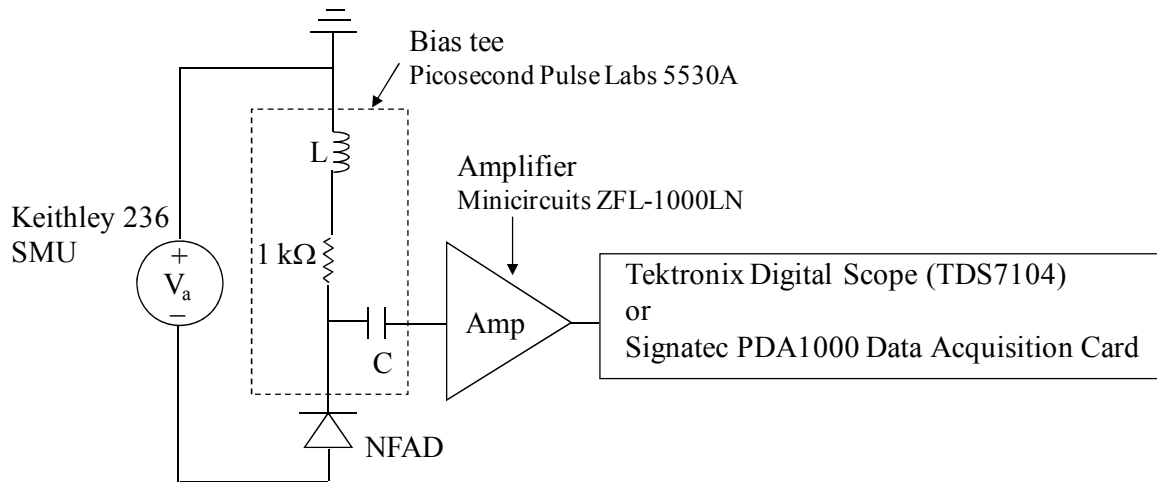


Figure 2. Schematic of test set-up for NFAD device characterization.

We have fabricated two iterations of NFAD devices. The resistances obtained from the first iteration devices range from 25 to 110 k Ω , depending on the device size. For the second iteration of NFAD devices, we achieved much higher resistances in the range of \sim 500 – 3000 k Ω . Devices from the two iterations show quite interesting differences in their performance. In the following section, we will focus on one device type (D3F7) from the first iteration and one device type (E4G8) from the second iteration. D3F7 and E4G8 are 1.55 μ m and 1.06 μ m NFADs, respectively. The optical active area diameters are 58 and 42 μ m for D3F7 and E4G8, respectively. The resistances of the integrated resistors on D3F7 and E4G8 are \sim 90 k Ω and 2.8 M Ω , respectively.

3. CHARACTERIZATION OF NFAD DEVICES

Given the capability of an data acquisition card with very deep memory, we can collect long data strings which contain many avalanche events (ranging from hundreds to more than one hundred thousand). From these long data strings, we can extract much useful information about avalanches in the NFADs. We are interested in parameters such as avalanche peak voltage, the amount of charge involved in avalanche events, interarrival time between adjacent pairs of avalanche events, etc. Information concerning the distribution of avalanche amplitudes is important for applications that make use of threshold voltage detection for avalanche discriminations. The distribution of charge flow per avalanche is important for understanding the quench and recovery dynamics, and for its relationship to the severity of afterpulsing effects. The interarrival time distribution contains information pertaining to the origin of avalanche counts, i.e., either from intrinsic dark or photo counts, or from afterpulsing. In D3F7, a persistent current phenomena was observed, the distribution of the amplitudes and periods of oscillations due to persistent current is helpful for understanding avalanche dynamics inside the APD. Finally, a photon counting measurement will show the viability of NFADs in real applications, and from these measurement the intrinsic photon detection efficiency of the device can be extracted as well.

3.1 NFAD avalanche pulses

Figure 3 shows some typical avalanche pulses from D3F7 under different bias voltages at 230 K. When an avalanche is triggered by either a dark carrier or a photo generated carrier, the avalanche quickly builds up and this shows up as the

negatively going sharp edge on Figure 3. As the avalanche current builds up, the monolithically integrated resistor will start to shift bias voltage away from the diode, and the bias voltage across the APD drops. When the overbias voltage is relatively low, the avalanche will be readily quenched, as shown in Figure 3(a). However, when the overbias voltage is relatively high, the APD will remain in a state with persistent current flow through it prior to quenching, as shown in Figure 3(b). We will discuss the persistent current issue later in this section. For E4G8, the quench resistance is so high, and persistent current was not observed at any overbias value used. Figure 4 shows a typical avalanche pulse for E4G8 at 230 K.

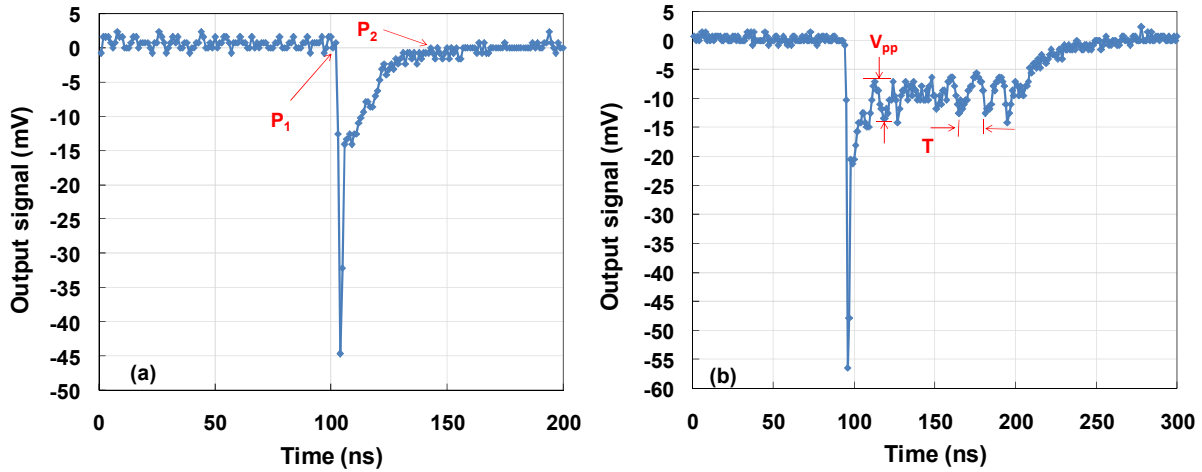


Figure 3. Avalanche pulses of D3F7 at 72.1 V (a) and 72.6 V (b) at $T=230$ K. In (a), P_1 is the point where the avalanche starts and P_2 is the point where the avalanche ends. In (b), V_{pp} is the peak to peak voltage of one oscillation peak in the persistent current mode, and T is the time interval between two oscillation peaks.

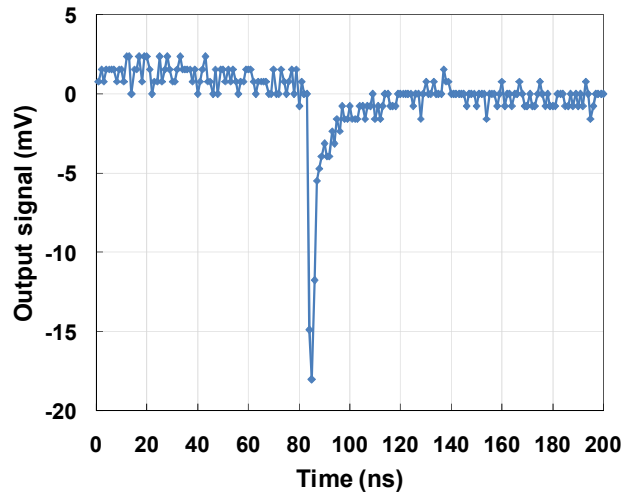


Figure 4. Avalanche pulses of E4G8 at 78.25V at 230 K.

3.2 Distribution of pulse heights

Figure 5 shows the normalized counts of avalanche pulse amplitudes for D3F7 (a) and E4G8 (b) at 230 K. The symbols are the experimental results. In Figure 5(a), the bias voltages for the blue and red symbols are 71.9 V and 72.6 V, respectively. In Figure 5(b), the bias voltages for the blue and red symbols are 78 V and 80.5 V, respectively.

As can be seen from Figure 5(a), when bias voltage is changed from 71.9 V to 72.6 V, the typical pulse height changes from 37 mV to 56 mV, which is proportional to the change of over bias voltage. However, in the case of Figure 5(b), when the bias voltage is changed from 78 V to 80.5 V, the typical pulse height remains the same with the change of over bias voltage of 2.5 V.

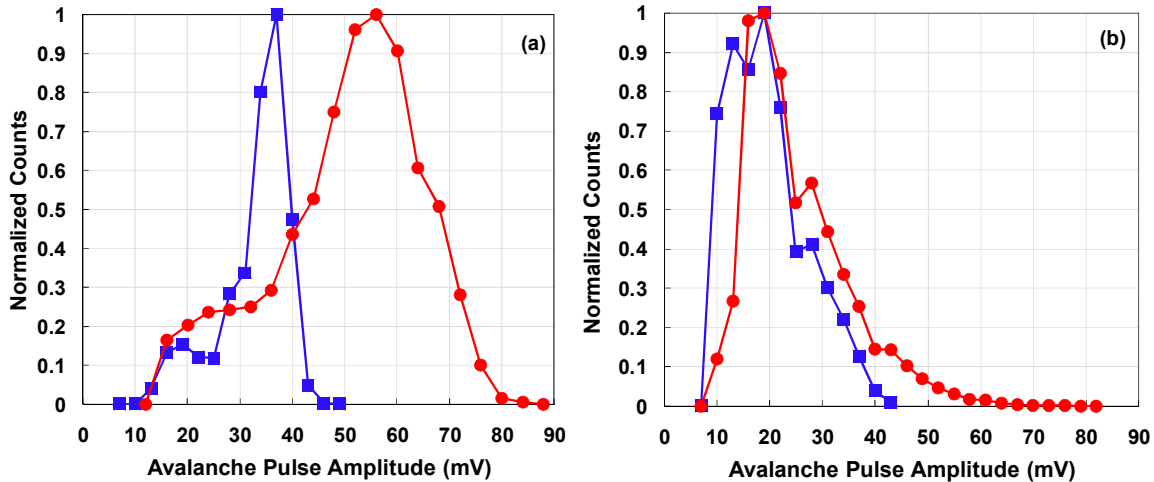


Figure 5. Normalized counts of avalanche pulse amplitudes for D3F7 (a) and E4G8 (b) at $T = 230$ K. In (a), squares and circles represent the results obtained with bias voltage of 71.9 V and 72.6 V, respectively. In (b), the squares and circles are obtained with bias voltages of 78 V and 80.5 V, respectively.

3.3 NFAD avalanche charge

Figure 6 shows the normalized counts of avalanche charges for D3F7 (a) and E4G8 (b) at 230 K. The unit of avalanche charge is e (the charge of a single electron). The avalanche charge is obtained as follows: first dividing the output voltage from the amplifier by its gain and 50Ω , then integrating the avalanche current from the time where avalanche starts (for example, P_1 in Figure 3(a)) and to the time where avalanche ends (for example, P_2 in Figure 3(a)).

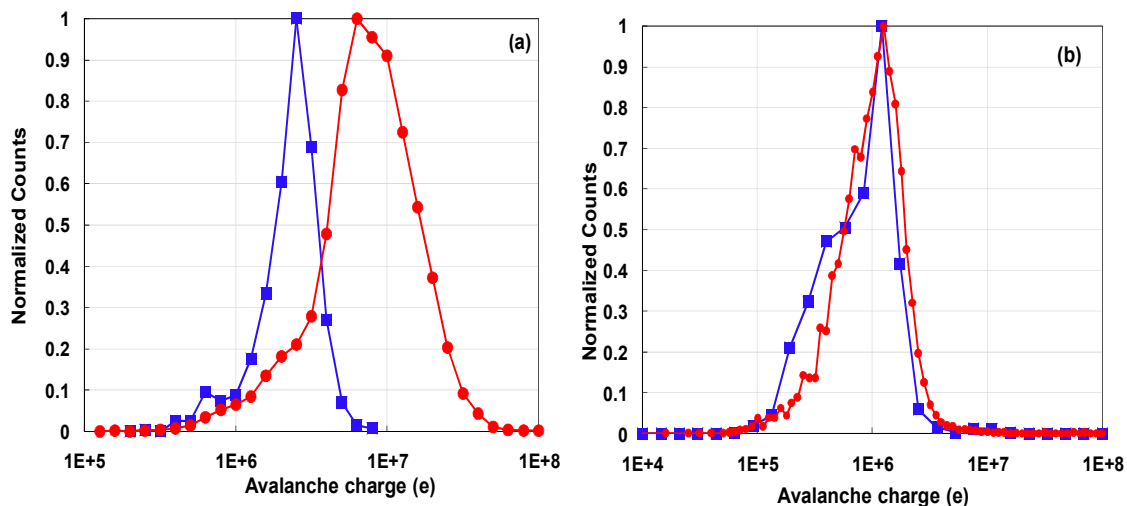


Figure 6. Normalized counts of avalanche charges for D3F7 (a) and E4G8 (b) at $T = 230$ K. In (a), squares and circles represent the results obtained with bias voltage of 71.9 V and 72.6 V, respectively. In (b), the squares and circles are obtained with bias voltages of 78 V and 80.5 V, respectively.

In Figure 6 (a) the squares are the result for 71.9 V, and the circles are for 72.6 V. In Figure 6(b) the squares are the result of 78 V, and the circles are the result for 80.5 V. For D3F7 at 230 K, the typical avalanche charge is 2.51×10^6 and 6.31×10^6 for bias voltage of 71.9 V and 72.6 V, respectively. For E4G8 at 230 K, the typical avalanche charge remains at 1.26×10^6 at both 78 V and 80.5 V. As in the case of the avalanche pulse amplitude distribution, we see a very different dependence of avalanche charge on overbias voltage in D3F7 and E4G8.

3.4 Interarrival time

Figure 7 shows the distribution of interarrival times between pairs of adjacent avalanche pulses in D3F7 (a) and E4G8 (b) at $T = 230$ K. In Figure 7(a), the blue and red symbols correspond to the bias voltage of 71.9 V and 72.6 V, respectively.

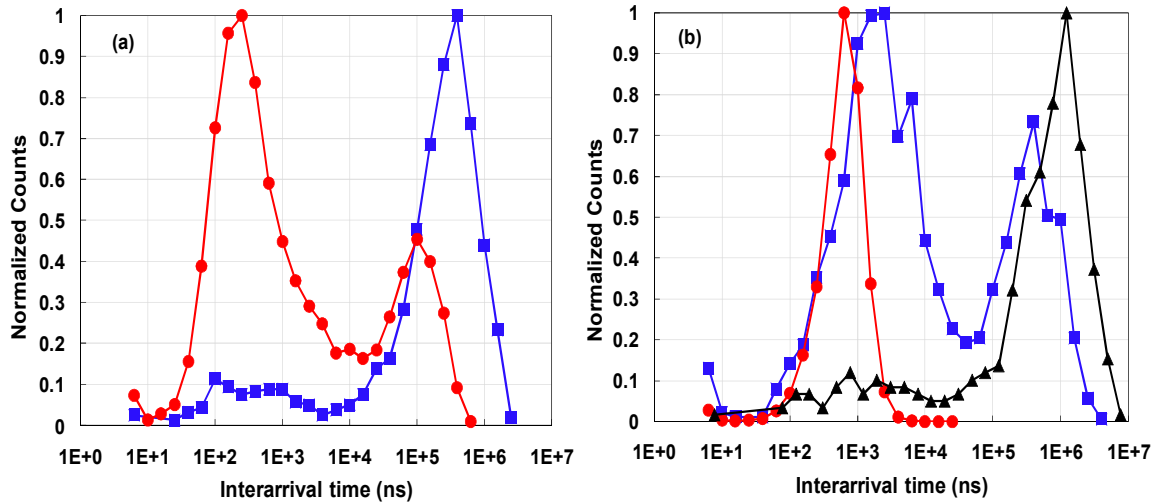


Figure 7. Normalized counts of interarrival time between two adjacent avalanche pulses for D3F7 (a) and E4G8 (b) at $T = 230$ K. In (a), blue squares and red circles correspond to bias voltages of 71.9 V and 72.6 V, respectively. In (b), black triangles, blue squares and red circles correspond to bias voltages of 77.2 V, 78 V and 80.5 V, respectively..

In Figure 7(b), the black, blue and red symbols correspond to the bias voltages of 77.2 V, 78 V and 80.5 V, respectively. For D3F7, at 71.9V bias voltage, the typical interarrival time is at 0.4 ms, and also there exists a broad shallow peak between 100 ns to 1 μ s. When bias is changed to 72.6 V, the peak is at about 250 ns, and there is a second peak at about 0.1 ms. A simple calculation shows after each avalanche the time for over bias voltage recovers to 95% of the initially applied value is ~ 135 ns. We believe that the peak at ms-scale interarrival times is due to intrinsic dark counts, whereas the peak at 100s of ns is due to afterpulsing. Similar phenomena can be seen on E4G8. When the bias voltage is at 77.2V, intrinsic dark counts dominate; when the bias voltage is at 78 V, we can see both intrinsic dark counts and afterpulsing. However, when the bias voltage is changed to 80.5 V, only afterpulses are seen. The peak value corresponding to intrinsic dark counts for 77.2 V and 78 V is 1.23 ms and 0.4 ms, respectively. The peak values corresponding to afterpulsing for 77.2V, 78 V and 80.5 V bias voltages are 776 ns, 2510 ns, and 631 ns, respectively. The time for over bias voltage to recover to 95% of its initial value is ~ 2500 ns.

3.5 Avalanche pulse height versus interarrival time

Figure 8 shows the avalanche pulse amplitude for the second pulse in a pair of adjacent avalanche pulses versus the interarrival time between the two pulses. The bias voltage for D3F7 is 72.6 V and that for E4G8 is 78 V. The temperature in both cases is 230 K. When the interarrival time is between ~ 10 ns to ~ 1 μ s, avalanche pulse amplitude changes significantly with interarrival time. This is due to the recovery time of the overbias voltage after each avalanche, and the counts here are most likely due to afterpulsing. In the time range of ~ 1 μ s to slightly less than 100

μs , the avalanche pulse amplitude changes only slightly with interarrival time. When the interarrival time is more than 0.1 ms, the avalanche pulse amplitude is relatively insensitive to interarrival time, and the counts observed in this range are most likely due to intrinsic dark counts. E4G8 shows similar behavior, i.e., avalanche pulse amplitude increases significantly with interarrival time in the range of ~ 50 ns to 10 μs , and is relatively insensitive to interarrival time when interarrival time is more than 0.1 ms. The counts observed in the two regions are due to afterpulsing and intrinsic dark counts, respectively. The results shown here are consistent with those of Figure 7.

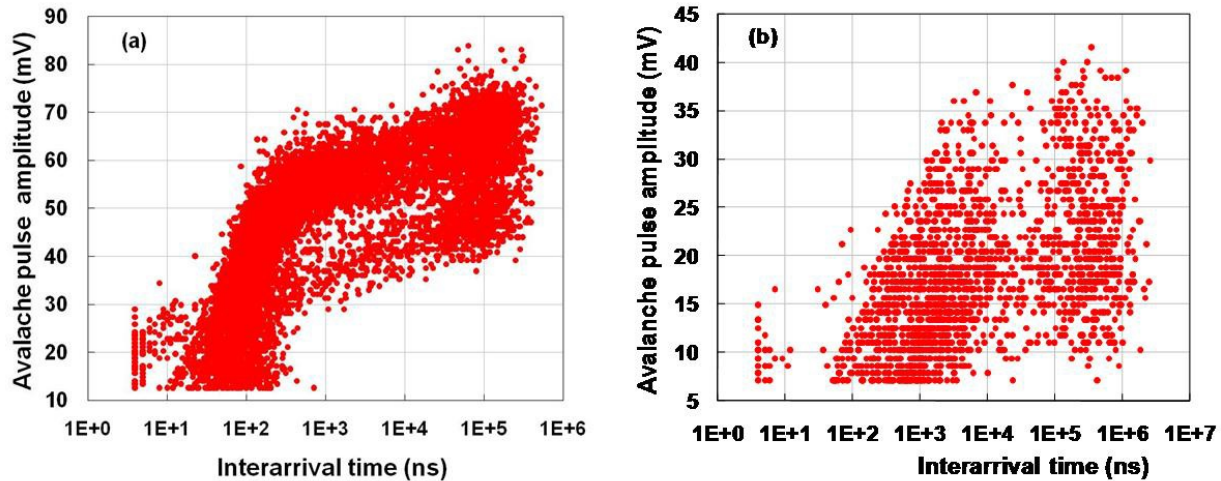


Figure 8 Avalanche pulse amplitude versus interarrival time for D3F7 at 72.6 V (a) and for E4G8 at 78 V (b). The temperature is 230 K.

3.6 Persistent current phenomena

As mentioned previously, persistent current phenomena is observed in D3F7, whereas it is not observed in E4G8. In the evolution of a GmAPD avalanche event, there is a steady state current, I_f , which depends on the overbias voltage, the total resistance of the intrinsic APD, and the quench resistor (integrated either monolithically or hybridly). To quench an avalanche, carriers must exit the multiplication region more rapidly than they are generated. There exists a characteristic latching current I_q such that when $I_f \ll I_q$, the avalanche has a high probability of quenching quickly. This is the situation for E4G8 at all overbias values used, whereas it is true for D3F7 only at very low overbias. When I_f is comparable to I_q , the carriers inside multiplication region fluctuate and the quenching of avalanche pulse becomes highly stochastic. Under this situation, there will exist a persistent current due to the fluctuation of carriers inside multiplication region and this is the case for D3F7 at relatively high overbias voltage.

In Figure 3(b), V_{pp} represents the peak of peak voltage of one oscillation peak (oscillation amplitude), and T is the time interval between two oscillation peaks (oscillation period). V_{pp} and T have some statistical fluctuation for different oscillation peaks, and Figure 9 shows the distribution of normalized counts for the oscillation amplitude (peak to peak) (a) and oscillation period (b) due to persistent current in D3F7 at 72.6 V and 230 K. The typical oscillation amplitude is ~ 5 mV, and the typical oscillation period is ~ 11 ns.

3.7 Photo detection efficiency

Figure 10 shows the dependence of detection probability of D3F7 on photon number per pulse, the temperature is 230 K. Simulated detection probability with photon detection efficiency changing from 2% to 7% are shown in solid curves. Experimental results for two over bias voltages, i.e., 0.2 V (blue squares) and 0.7 V (red circles) are shown there as well. The intrinsic photon detection efficiencies for 0.2 V and 0.7 V over bias voltage were extracted to be 3% and 7%, respectively, which agree reasonable well with simulated results.

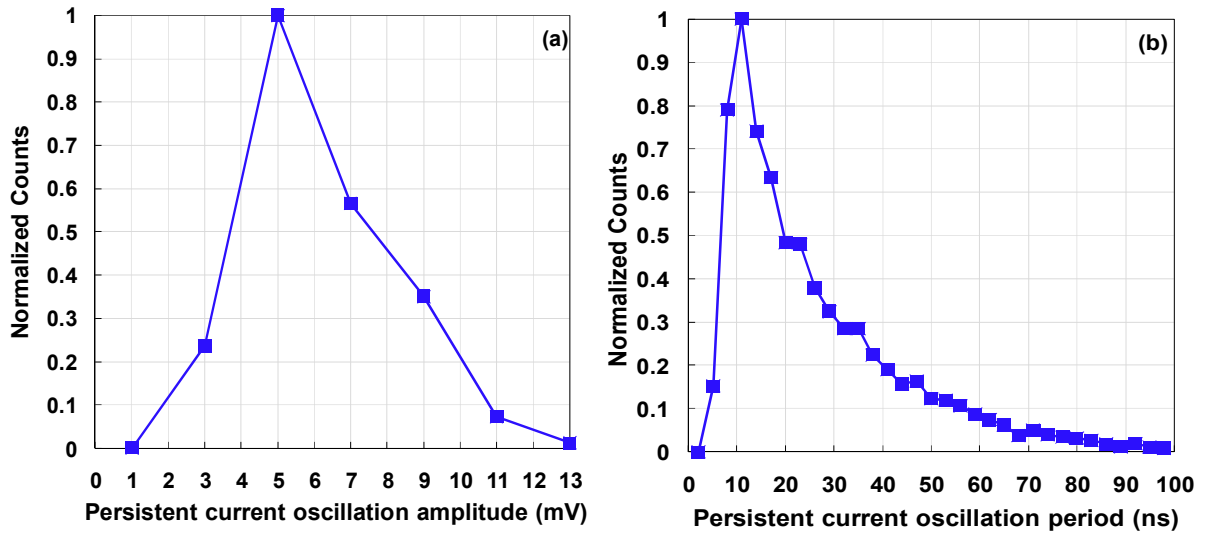


Figure 9 Normalized counts for persistent current oscillation amplitude (a) and oscillation period (b) in D3F7 at 72.6 V and 230 K.

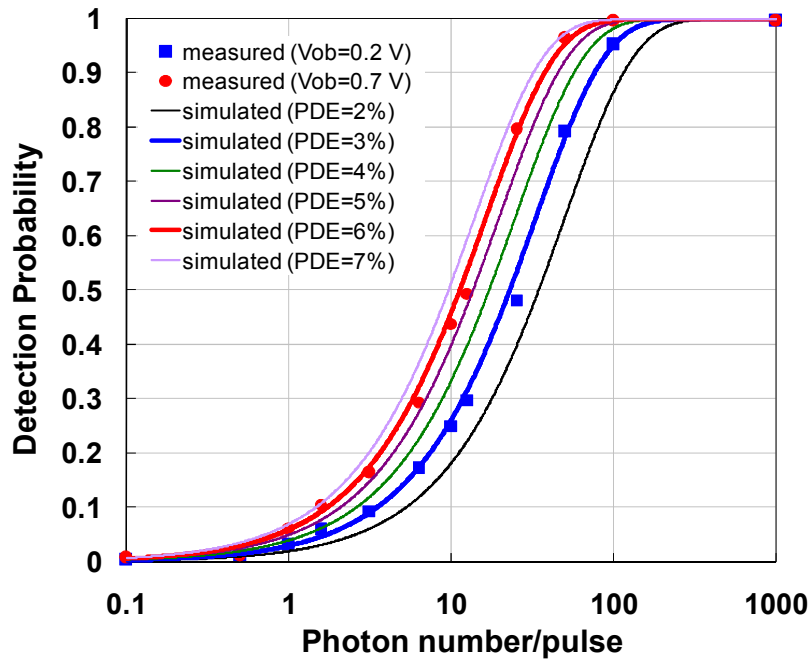


Figure 10. Dependence of detection probability of D3F7 on photon number per pulse. The measured data were taken at overbias voltage of 0.2 V (squares) and 0.7 V (circles), respectively. The simulated results increases from 2% to 7% with a step size of 1%.

4. DISCUSSIONS AND CONCLUSIONS

Two NFAD devices, D3F7 and E4G8, show some similarity in performance, but also show some striking differences. In D3F7, the avalanche pulse amplitude changes in proportional to over bias, as expected, and the charge flow per avalanche event changes with overbias voltage as well. However, in E4G8, both the avalanche pulse amplitude and

avalanche charge are insensitive to the overbias voltage. The monolithically integrated resistor in D3F7 behaves as a typical quenching resistor. In contrast, E4G8 exhibits behavior that seems to qualitatively differ from standard passive quenching, i.e. the integrated resistance not only quenches avalanches after they are generated, but it also seems to regulate the avalanche generation from the very onset of the avalanche process.

Persistent current was observed in D3F7 when the overbias voltage was increased to a sufficiently high value. A similar phenomena was not observed in E4G8. The much larger resistance in E4G8 caused the steady state current I_f in E4G8 to be much lower than the latching current I_q , and quenches the avalanche process very rapidly. Persistent current is detrimental to detector performance since it results in larger charge flow through the device. Moreover, while carrying persistent current, the device is not armed for the detection of incident photons. However, the persistent current phenomena provides a useful way to study the carrier dynamics within the multiplication region. The typical oscillation amplitude and period of the persistent current state provide useful information for further study.

The NFAD device significantly reduces the charge flow in the avalanche event compared to that of the regular SPAD. However, even at the $10^5 - 10^6$ carrier level, afterpulsing is still an issue. As can be seen from Figures 7 and 8, when the overbias voltage is increased, the afterpulsing quickly shows up in addition to the intrinsic dark counts. As presently designed, this may constrain the operation of NFADs to lower overbias voltage where afterpulsing is insignificant. However, these NFAD devices will be useful in applications where relatively high incident photon flux is present, as demonstrated in Figure 10.

In conclusion, we have presented the results of NFAD devices from two different iterations. These NFAD devices show performance benefits compared to the regular SPADs, such as reduced charge flow per avalanche event, improved uniformity in pulse heights and avalanche charge flow, and the potential to resolve photon number when put into a matrix format. Moreover, because the NFADs are self-quenching, they can be operated with just a DC bias voltage and very simple back-end detection electronics, in contrast to the rather complex arming and quenching circuitry required by standard SPADs. NFADs also show some interesting phenomena that have not been seen in SPADs, such as the persistent current in D3F7 and insensitivity to overbias voltage as seen in E4G8. These devices are not only useful photodetectors, but also provides a unique way to study the device physics and carrier dynamics in APDs.

Acknowledgement—This work was supported in part by NASA/GSFC and JPL. Discussions with Bill Farr and Michael Krainak on the NFAD concept and characterization are greatly appreciated.

REFERENCES

1. B. F. Levine, C. G. Bethea and J. C. Campbell, "Room temperature 1.3- μm optical time reflectometer using a photon counting InGaAs/InP avalanche detector", *Appl. Phys. Lett.* 46(4), 333-335 (1985).
2. N. Gisin, G. Ribordy, W. Tittel and H. Zbinden, "Quantum cryptography", *Rev. Mod. Phys.* 74(1), 145-195 (2002).
3. R. G. W. Brown, K. D. Ridley and J. G. Rarity, "Characterization of silicon avalanche photodiodes for photon-correlation measurements. I: Passive quenching", *Appl. Opt.* 25(22), 4122-4126 (1986).
4. J. G. Rarity and P. R. Tapster, "Experimental violation of Bell's inequality based on phase and momentum", *Phys. Rev. Lett.* 64(21), 2495-2498 (1990).
5. A. L. Lacaíta, F. Zappa, S. Bigliardi and M. Manfredi, "On the bremsstrahlung origin of hot-carrier-induced photons in silicon devices", *IEEE Trans. Electron Devices* 40(3) 57-82 (1993).
6. R.M. Measures, *Laser Remote Sensing – Fundamentals and Applications*, John Wiley & Sons, 1984.
7. Special issue on "Free-space communication techniques for optical networks", *IEEE LEOS Newsletter* 19 (5), 6-39 (2005).
8. V.E. Shubin and D.A. Shushakov, "New avalanche device with the ability of analog few-photon pulse detection", *Proc. of the SPIE* 2550, 284 – 293 (1995).
9. D. Bisello, Yu. Gotra, V. Jejc, V. Kushpil, N. Malakhov, A. Paccagnella, Z. Sadygov I. Stavitsky and E. Tsyganov, "Silicon avalanche detectors with negative feedback for high energy physics", *Nuclear Instruments and Methods in Physics Research A* 367, 212 – 214 (1995) .
10. K. Zhao, A. Zhang, Y.-h. Lo and W. Farr, "InGaAs single photon avalanche detector with ultralow excess noise", *Appl. Phys. Lett.* 91(8), 081107 (2007).

11. M.A. Itzler, X. Jiang, B. Nyman and K. Slomkowski, "InP-based negative feedback avalanche diodes", *Proc. of the SPIE* 7222, 72221K (2009).
12. S. Cova, M. Ghioni, A. Lacaita, C. Samori and F. Zappa, "Avalanche photodiodes and quenching circuits for single-photon detection", *Appl. Opt.* 35(12), 1956–1976 (1996).
13. M.A. Itzler, R. Ben-Michael, C.-F. Hsu, K. Slomkowski, A. Tosi, S. Cova, F. Zappa and R. Ispasoiu, "Single photon avalanche diodes (SPADs) for 1.5 μ m photon counting applications", *J. Modern Optics* 54 (2-3), 283 – 304 (2007).
14. M.A. Itzler, X. Jiang, R. Ben-Michael, K. Slomkowski, M.A. Krainak, S. Wu and X. Sun, "InGaAsP avalanche photodetectors for non-gated 1.06 μ m photon-counting receivers", *Proc. of the SPIE* 6572, 65720G (2007).
15. X. Jiang, M. A. Itzler, R. Ben-Michael, and K. Slomkowski, "InGaAsP–InP Avalanche Photodiodes for Single Photon Detection", *IEEE J. of Sel. Topics in Quantum Electronics* 13(4), 895-905 (2007).